










Submitted: 03/07/2023

Accepted: 15/08/2023

Published: 30/09/2023

Inflammatory cell responses in biliary mucosa during *Opisthorchis viverrini* infection: Insights into susceptibility differences among hosts

Theerayut Thongrin¹ , Watcharapol Suyapoh² , Woro Danur Wendo¹ , Prasarn Tangkawattana¹ ,
Peerapol Sukon¹ , Kanin Salao³ , Sutas Suttiwapa^{3,4} , Prasert Saichua^{3,4}  and
Sirikachorn Tangkawatana^{1,4*} 

¹Faculty of Veterinary Medicine, Khon Kaen University, Khon Kaen, Thailand

²Faculty of Veterinary Science, Prince of Songkla University, Songkhla, Thailand

³Faculty of Medicine, Khon Kaen University, Khon Kaen, Thailand

⁴Tropical Disease Research Center, WHO Collaborating Centre for Research and Control of Opisthorchiasis, Khon Kaen University, Khon Kaen, Thailand

Abstract

Background: Individual host susceptibility is believed to be a risk factor in the interaction between the host and the parasite. Since studying time series in humans is limited, animal models are replaced.

Aim: This study aims to explore and compare the pattern of inflammatory cell types along the biliary tract and their association with proliferative lesions in the early development of cholangiocarcinoma from susceptible and nonsusceptible animal models.

Methods: Thirty male Syrian golden hamsters and 30 BALB/c mice, serving as the susceptible and nonsusceptible animal models, were used in this comparative study. The animals were infected with 50 *Opisthorchis viverrini* metacercariae via gastric intubation. At days 1, 2, 7, 14, 28, and 56 postinfection (p.i.), five animals were randomly selected from each group and humanely sacrificed. The hepatobiliary tissues were collected and processed for histopathological study. Histochemical and immunohistochemical staining were applied to differentiate the inflammatory cell types. Kruskal–Wallis and Mann–Whitney tests were applied to assess all semi-quantitative and quantitative variables. The correlation between each variable was also analyzed using Spearman rank at a p -value < 0.05 .

Results: The results demonstrated that mice had different patterns of infiltrating cell types when compared to hamsters. This suggested that the cellular response to the infection in mice occurred earlier than that in hamsters. The response in mice reached its peak at D7 to D14 and then rapidly declined at D28. In contrast, although the inflammatory response in hamsters started slowly, the response reached the peak at D28 and maintained a high level until D56. Significant differences in the number of inflammatory cells between mice and hamsters were seen at D1 ($p = 0.047$), D7 ($p = 0.049$), D28 ($p = 0.040$), and D56 ($p < 0.040$).

Conclusion: The inflammatory responses to *O. viverrini* infection in the nonsusceptible animal model occurred and declined earlier while the response in the susceptible animal model occurred later in a gradual manner. Both rodents are suitable animal models for the studies of opisthorchiasis susceptibility.

Keywords: Inflammatory cells, Biliary, Proliferation, *Opisthorchis viverrini*, Susceptible and nonsusceptible host.

Introduction

Bile duct cancer, also known as cholangiocarcinoma (CCA), is a significant public health problem in Southeast Asia due to its link to the food culture of people living in water reservoirs. Host immunity in *Opisthorchis viverrini* (*O. viverrini*) infection begins with innate immunity and is strengthened by adaptive immunity. The interaction between host and parasite usually manifests in an inflammatory response. The causative agent, *O. viverrini*, can stimulate and enhance cancer development through the inflammation process.

However, not all individuals infected with *O. viverrini* develop CCA, with less than 1% of patients taking the risk (Mairiang, 2017). It has been observed from the community study that individuals who have a strong, reactive response to the worm are often diagnosed with CCA (Sripa et al., 2018a).

Inflammation serves as an important host defense mechanism that prevents causative agents from harming the host. In opisthorchiasis, both innate and adaptive immunity respond subsequently to the parasite antigens that stimulate throughout the infection. However, the

*Corresponding Author: Sirikachorn Tangkawatana. Faculty of Veterinary Medicine, Khon Kaen University, Khon Kaen, Thailand. Email: sirikach@kku.ac.th

effects of the inflammatory response are believed to lead to genetic damage and ultimately develop CCA (Sripa et al., 2018a). Infection with *O. viverrini* stimulates both antibody and cellular responses to its *O. viverrini* and ES antigens. The parasite products and resulting tissue damage encourage innate and adaptive immune responses after infection. Inflammatory cells, such as neutrophils and eosinophils, are involved in the acute phase, followed by mononuclear cells in the later and chronic phases, as well as periductal (Sripa and Kaewkes, 2000a; Pinto et al., 2018; Upontain et al., 2018). Recent studies in a hamster model showed that infection with *O. viverrini* with or without *Helicobacter pylori* resulted in a significant change in the number of inflammatory cells (Suyapoh et al., 2021a, 2021b). The difference in host response may be due to the different antigenic recognition of B cells, which reflects the antibody response pattern (Watakulsin et al., 2023). The presence of liver fluke antigens and damaged tissue continuously stimulates immune and inflammatory responses from the acute to the chronic phase, ultimately leading to fibrotic changes in the biliary tract and liver (Prueksapanich et al., 2018; Sripa et al., 2018a).

Because studying susceptible and nonsusceptible people is limited, animal models are often used for investigation. The Syrian golden hamster (*Mesocricetus auratus*) is a susceptible animal model that has been commonly used in fluke and CCA studies (Boonmars et al., 2009; Wonkchalee et al., 2012). In addition, BALB/c mice were selected as the nonsusceptible animal model because the liver fluke could not establish the infection in this host (Uddin et al., 2012; Sripa et al., 2018a). Studies using the Syrian golden hamster model have shown that chronic infection with *O. viverrini* can lead to modulation of the immune response, which can contribute to the development of CCA. In particular, an increase in the immune response to *O. viverrini* antigens is associated with an increased risk of developing CCA (Sripa et al., 2018b). This suggests that immune modulation and dysregulation play a critical role in the pathogenesis of CCA. The BALB/c mouse model is widely used in studies of the immune response to parasitic infection; however, this strain of mice is resistant to the establishment of *O. viverrini* in the biliary system. The worms are expelled before reaching maturity in the bile duct, typically within 3–4 weeks after infection (Kaewkes et al., 1991). Therefore, we aimed to investigate the inflammatory cell types infiltrating along the biliary tract and their association with the proliferative lesions in the pathogenesis of CCA comparing the susceptible host (Syrian golden hamster) and nonsusceptible host (BALB/c mouse) model.

Materials and Methods

Animal models: susceptible/nonsusceptible models

Male Syrian golden hamsters and male BALB/c mice, aged 6–8 weeks, were used as susceptible and

nonsusceptible animal models, respectively. All rodents were housed in the Laboratory Animal Unit of the Faculty of Medicine and the Northeast Laboratory Animal Center at Khon Kaen University and provided with *ad libitum* access to commercial pellet food and clean water. Thirty hamsters and 30 BALB/c mice were used in this study, with each animal model equally divided into two groups: an *O. viverrini*-infected group and a control group. Each animal in both models was infected with 50 *O. viverrini* metacercariae by gastric intubation or served as a normal control group (noninfected group). To evaluate the effects of infection, five animals from each group were designated for sacrifice at D1, D2, D7, D14, D28, and D56 postinfection (p.i.), respectively. The animals were then euthanized using isoflurane inhalation methods. The fecal examination was performed using a modified formalin-ether concentration technique (FECT) method previously described (Kopolrat et al., 2022), and the morphology of the *O. viverrini* egg was observed. Identification of the egg was based on previous studies (Kaewkes et al., 1991; Sanpool et al., 2018), which included observations of an operculated egg, a knob at the contrary of the operculum, a rough surface eggshell, and a completely matured miracidium. Liver and biliary tracts were dissected and preserved in 10% buffered formalin and routinely processed for histopathological, histochemical, and immunohistological studies.

Histopathological and histochemical studies and grading evaluation

Histopathological and histochemical studies were performed, and grading evaluation was conducted on the biliary tract in all animals using H&E histological slides. The histopathological evaluation was modified from (Lvova et al., 2012) to compare the susceptible and nonsusceptible animal models based on the following criteria (Table 1): overall inflammatory cell infiltration and investigation of the cell type, such as neutrophil, eosinophil, and mast cell, and mononuclear cells such as T-lymphocyte, B-lymphocyte, and macrophage. In addition, biliary proliferation lesions (such as bile duct proliferation, hyperplasia, and dysplasia) were investigated. Histochemical staining such as alcian blue-safranin O staining (Abcam, UK) was applied for mast cell identification and Sirius red for fibrosis demonstration (Ishak et al., 1995; Grigorev and Korzhevskii, 2021). Other inflammatory cells, such as T lymphocyte, B lymphocyte, and macrophage, were further examined using immunohistochemical techniques.

Immunohistochemical studies for CD3 IHC, CD79a and macrophage

Based on Sirivisoot et al. (2018), immunohistochemistry (IHC) was used to identify types of inflammatory cells, such as T-lymphocytes, B-lymphocytes, and macrophages, as described below.

Immunohistochemistry for T lymphocyte (CD3)

Immunohistochemistry was performed to detect T-lymphocytes using CD3 as a marker. The deparaffinization

Table 1. Quantitative and semi-quantitative gradings of main histopathologic features and the BrdU index in rodent livers.

| No. | Point | Criteria | References |
|-----|---|--|--|
| 1 | Total inflammatory cell infiltration grades | Grades 0 = 0%–1%, 1 = 2%–25%, 2 = 26%–50%, and 3 = >50% of distribution per area of the specimen | Lvova et al. (2012) |
| 2 | PDF grades | 0 = no fibrosis 1 = mild fibrous expansion of some portal areas 2 = moderate fibrous expansion of most portal areas with short fibrous septa 3 = severe fibrous expansion of most portal areas with occasional portal to portal bridging 4 = more severe fibrous expansion of most portal areas with marked bridging | Ishak et al. (1995); Sharma et al. (2011) |
| 3 | CD3, CD79a, and macrophage | Quantitative data | Sirivisoot et al. (2018) |
| 4 | Proliferation (BrdU) BrdU index (%) = positive biliary cells*100/total 1,000 biliary cells | 0 = Number of positive biliary cell is less than 1% of total biliary cells 1 = Number of positive biliary cell is 1%–25% of total biliary cells 2 = Number of positive biliary cell is 25%–50% of total biliary cells 3 = Number of positive biliary cell is 50% of total biliary cells | Lvova et al. (2012) |

and rehydration steps followed the protocol described above. Antigen retrieval for CD3 was achieved by heating tissue in 0.1 M sodium citrate (pH 7.6) using a high-pressure cooker for 10 minutes. After blocking with 5% normal horse serum for 30 minutes, tissue sections were incubated overnight at room temperature with monoclonal rabbit anti-CD3 (dilution 1:200, ab16669, Abcam plc, Cambridge, UK). Subsequently, sections were incubated with goat anti-rabbit IgG H&L (HRP) (dilution 1:200, ab205718, Abcam plc, Cambridge, UK) for 1 hour at room temperature. The reaction was visualized using 0.03% 3,3'-diaminoperoxidase (DAB) mixed with H₂O₂, followed by counterstaining with Mayer's hematoxylin. After rinsing with tap water, sections were dehydrated in graded alcohol and mounted with Permount (Thermo Fisher Scientific, UK). Normal spleen and normal liver tissue were used as positive and negative controls for CD3, respectively.

Immunohistochemistry for B lymphocyte (CD79a)

Immunohistochemistry was performed to detect B-lymphocytes using CD79a as a marker. The staining protocol was similar to that used for CD3 IHC but utilized EnVision Detection Systems. Tissue sections were incubated overnight at room temperature with monoclonal rabbit anti-CD79a antibody (dilution 1:200, CD79a (D1X5C) XP® Rabbit mAb#13333, Cell Signaling®, USA). The sections were then incubated with EnVision Kit (#K5007-11, EnVision Detection Systems Peroxidase/DAB, Rabbit/Mouse, DAKO®,

USA) for 1 hour at room temperature before following the step of color development, counterstain, rehydration, and mounting. Positive and negative control tissues for CD79a expression were normal spleen and liver tissue, respectively.

Immunohistochemistry for macrophage

The staining protocol was similar to that used for CD3 and CD79a, but antigen retrieval was performed by heating the tissue in 0.1M EDTA. Tissue sections were incubated with monoclonal rat anti-macrophage antibody (dilution 1:200, ab56297, Abcam plc, Cambridge, UK) overnight at room temperature. After washing, the sections were incubated with goat anti-rat IgG H&L (ab205720, Abcam plc, Cambridge, UK) for 1 hour at room temperature. Positive and negative control tissues were normal spleen tissue from hamsters and mice and normal liver tissue from hamsters and mice, respectively.

Immunohistochemistry for cell proliferation (BrdU IHC)

At least 30 minutes before euthanasia, the animals were injected with 0.01 mg/ml 5-bromodeoxyuridine (BrdU) intraperitoneally to let the chemicals cooperate to host DNA. The immunohistochemical staining was similar to those in CD3 IHC. deparaffinization and rehydration steps were similar to those previous methods. The primary and secondary antibodies used were polyclonal sheep anti-Bromodeoxyuridine (dilution 1:500, ab1893, Abcam plc, Cambridge, UK), at room temperature overnight.

Then, the sections were incubated by biotinylated rabbit anti-sheep IgG (dilution 1:200, ab97130, Abcam plc, Cambridge, UK) for 1 hour at room temperature. Positive and negative controls for BrdU were hamster CCA and normal hamster/mouse liver tissue.

Data evaluation and analysis

Histopathology evaluation

The pathological observation was diagnosed and confirmed by 2 pathologists. The acute phase of infection was defined as days 1, 2, 7, and 14 postinfection with immature *O. viverrini*, while the chronic phase was defined as days 28 and 56 postinfection with mature worms. Slides were examined for biliary lesions, and the pathological outcomes for each treatment were described qualitatively and graded semi-quantitatively based on the following criteria: inflammation, hyperplasia, and dysplasia of the bile duct or cholangiocyte, which were graded based on a modified grading system from Lvova et al. (2012). Periductal fibrosis (PDF) was also graded based on a modified grading system from Ishak et al. (1995) and Sharma et al. (2011) (Table 1).

Immunohistochemical grading

The immunohistochemical staining of CD3, CD79a, and macrophage was evaluated using a semi-quantitative grading system modified by Zhao et al. (2020). The grading system was based on the percentage of positively stained cholangiocytes per counted cholangiocytes and the distribution of staining. The percentage of positively stained cells was graded as described in Table 1. The proliferation activity of biliary cells from BrdU immunohistochemistry was modified by Lvova et al. (2012). The conclusion of the criteria in detail is shown in Table 1.

Statistical analysis

Statistical analysis was performed using SPSS version 26.0 software (SPSS Inc., USA). The Kruskal–Wallis test and Mann–Whitney *U* test were used to evaluate semi-quantitative variables including the number of mast cells, neutrophils, eosinophils, T lymphocytes, B lymphocytes, and macrophages. For ordinal-level data, the Spearman rank order correlation was used to measure the direction and strength of the association between bile duct inflammatory cells, and PDF grades. A *p*-value less than 0.05 was considered statistically significant. To account for skewed distributions that have outliers, the interquartile range (IQR) was used as a measure of variance. This measure is based on the middle half of the distribution, which is not affected by outliers.

Ethical approval

The study was approved by the Animal Ethics Committee of Khon Kaen University in accordance with the Ethics of Animal Experimentation of the National Research Council of Thailand (ACUC KKU 78/2561 and 35/2563).

Results

Both laboratory animal models, representing responsive and nonresponsive models of *O. viverrini*

infection were studied histopathologically. The study focused on two clusters of biliary lesions: types of infiltrative inflammatory cells and biliary proliferative lesions, such as hyperplasia of the first and second order bile ducts, from the beginning of infection to D56 postinfection (p.i.). Before euthanasia, animal feces were collected to confirm the infection status using modified FECT. Stool examination reveals *O. viverrini* eggs were detected only in the hamster model on D28 (2 of 3, 66.67%) and D56 (3 of 3, 100%). In contrast, no egg was detected in a mouse model during periods. The results revealed that all hamsters and BALB-c mice in both infection and normal control groups showed no abnormal signs. Unfortunately, two hamsters from D28 and D56 died from fighting. A gross examination of the liver in the *O. viverrini*-infected group showed a slight enlargement. The liver of infected hamsters from D28 and D56 showed a thickening of the bile duct wall. Similarly, the cut surface revealed a thickening of the periductal area in the hepatic parenchyma. The opacity of the common bile duct and gall bladder increased in *O. viverrini*-infected hamsters on D56, but not in mice. Under the microscope, the infected liver of both animal models showed infiltration of inflammatory cells which was scarcely seen in the liver from normal control animals (Supplementary Tables S1 and S2). Histopathological examination revealed the presence of juvenile and dead worms in the liver section of mice at D14 and D28 p.i. Infiltration of inflammatory cells, which were investigated for each cell type, began from D1 to D56 p.i. A summary of the key study results is shown in Figure 1.

Inflammatory bile duct responses to *O. viverrini* infection compare between types of rodents and time periods

Inflammatory cell infiltration was observed in both rodent models that infiltrated along the portal triad or periductal area throughout the entire experiment (D1–D56). Mononuclear cells (lymphocytes, plasma cells, and macrophages) were the major population of infiltrating cells, particularly in the chronic phase. The infiltration was first observed predominantly around the first-order bile ducts and later extended to the second-order bile ducts. The overall inflammation grade was higher in the hamster groups with *O. viverrini* infection compared to the mice groups (Fig. 2a-iii). In the mouse model, the degree of inflammation was higher in the early period or acute phase compared to the chronic phase. Microscopic examination of the mouse model showed a predominant increase in inflammatory cells from the first day of infection, reaching a maximum level on D7 to D14 (grade 2; more than 500 cells/high-power field (HPF)), then gradually declining until D56. In contrast, in the hamster model, inflammatory cells had infiltrated the portal area since D1 and gradually increased to a maximum level on D28 (grade 3; around 1,400 cells/HPF),

then moderate-high population was maintained toward the chronic phase on D56 (grade 2). The hamster model showed a significantly higher number of inflammatory cells compared to the mouse model at D1 ($p = 0.047$), D7 ($p = 0.049$), D28 ($p = 0.040$), and D56 ($p = 0.040$). Each type of infiltrating inflammatory cell from the acute to chronic phase was counted, and semi-quantitative scores of overall inflammation are listed in Table 2. Neutrophils were the first cell type to infiltrate the infected liver in all groups and then declined. Eosinophils were the second cell population infiltrated around bile ducts and intraepithelial sites. Mononuclear cells were prominent in the chronic phase. The details of the inflammatory cell infiltration in this study are described as follows.

Infiltration of neutrophils

The histopathological study revealed that neutrophils were the first inflammatory cells to infiltrate the infected liver and biliary system, with initial infiltration often seen from the portal area. Although a small number of neutrophils were observed throughout the infection periods, they were mainly seen in the submucosa (Fig. 2bi–ii), while other inflammatory cell types were detected in the portal area. Comparing the two rodent models, neutrophil infiltration in the hamster reached the highest amount at D28 and then decreased at D56, while in mice, the increase was observed from D7 and peaked at D14. The number of neutrophils was significantly higher in the hamster than in the mice at D28 postinfection ($p = 0.039$) and D56 ($p = 0.005$). In

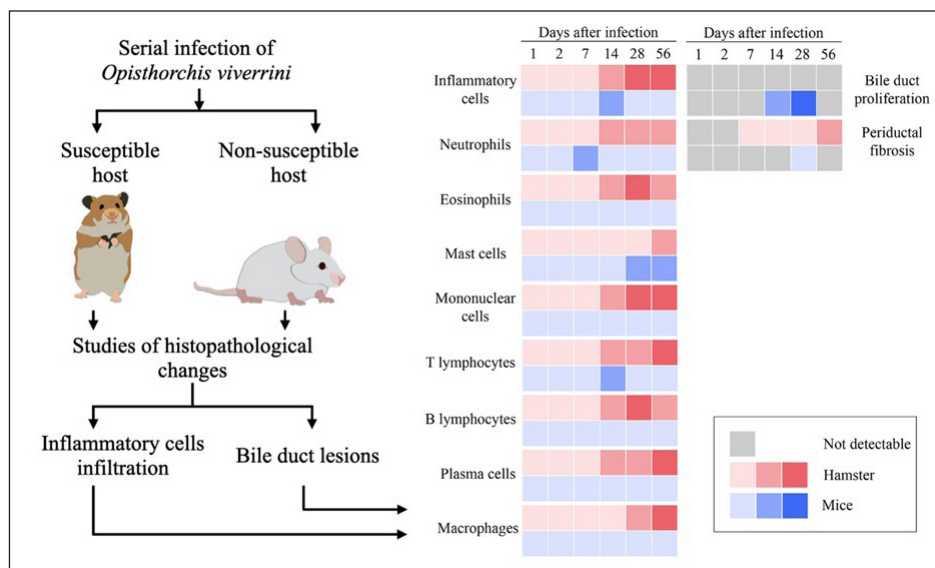


Fig. 1. The heat map illustrates the profile of inflammatory patterns, bile duct proliferation and PDF in susceptible and nonsusceptible animal models of opisthorchiasis.

Table 2. Comparison of inflammatory cell infiltration in hepatic parenchyma between mouse and hamster models infected with *O. viverrini*.

| Outcomes | Mice (MOV) (n = 90) | | Hamsters (HOV) (n = 66) | | p-value |
|-------------------|------------------------|--------------|----------------------------|--------------|---------|
| | Mean rank | Median (IQR) | Mean rank | Median (IQR) | |
| Neutrophils | 76 | 19 (1–41) | 83 | 21 (7–45) | 0.341 |
| Eosinophils | 76 | 2 (0–62) | 82 | 3 (0–142) | 0.410 |
| Mast cells | 64 | 0 (0–28) | 98 | 15 (3–48) | <0.001 |
| Mononuclear cells | 68 | 46 (9–105) | 93 | 89 (26–189) | <0.01 |
| T lymphocytes | 71 | 41 (8–156) | 88 | 122 (27–370) | <0.05 |
| B lymphocytes | 66 | 0 (0–3) | 95 | 3 (0–20) | <0.001 |
| Macrophages | 56 | 0 (0–0) | 108 | 8.5 (1–20) | <0.001 |

IQR: interquartile range.

*p-value from Mann–Whitney test.

contrast, the levels of neutrophil infiltration in mice with *O. viverrini* (OV) infection abruptly declined at D28 and D56 (Fig. 2biii).

Infiltration of eosinophils

Eosinophils were observed in the portal area, intra-epithelium, and submucosa of the biliary system, particularly in the intrahepatic bile ducts of infected animals (Fig. 2bi and ii). In hamsters, a high number of eosinophils were detected in the later period of infection (D28–D56). In contrast, in mice, a high number of eosinophils were detected at D7 and D14 and then declined by D28, reaching zero by D56. Semi-quantitatively, the eosinophil infiltration in hamsters was significantly higher than in mice at D28 ($p = 0.006$) and D56 ($p = 0.003$) postinfection (Fig. 2biv).

Infiltration of mast cells

Mast cell populations were mainly located in the submucosal area of biliary tracts. The cells were commonly detected in the common bile ducts and gall bladders of noninfected control of both rodents, which were rich in collagen fiber structure (Fig. 2ci and ii). In the mouse model, a higher number of mast cells

were detected in small amounts in the early period and increased on D14, reaching the maximum point at D56 with more fibrosis. In hamsters, the maximum number of mast cell infiltrations was found on the first day of infection, followed by a decline on D2, D7, and D14 before climbing up again on D28 and declining on D56 (Fig. 2ciii). A significantly higher mast cell infiltration was found in hamsters than in mice on D1, D2, and D3.

Infiltration of T lymphocytes

Using immunohistochemical techniques to demonstrate T lymphocytes, the results revealed differences between the animal models (Fig. 3bi and ii). In the mouse model, it was clear that the number of T lymphocytes gradually increased until D14, then declined close to zero on D56. A different trend was found in the hamster model, where the number of T lymphocytes fluctuated (up and down) (Fig. 3biii). T lymphocytes were higher in the mouse model on D7 ($p = 0.046$), but lower on D28 ($p = 0.003$), and particularly on D56 ($p = 0.000$).

Infiltration of B lymphocytes

B lymphocytes are a component of the mononuclear cell population, and their identification requires

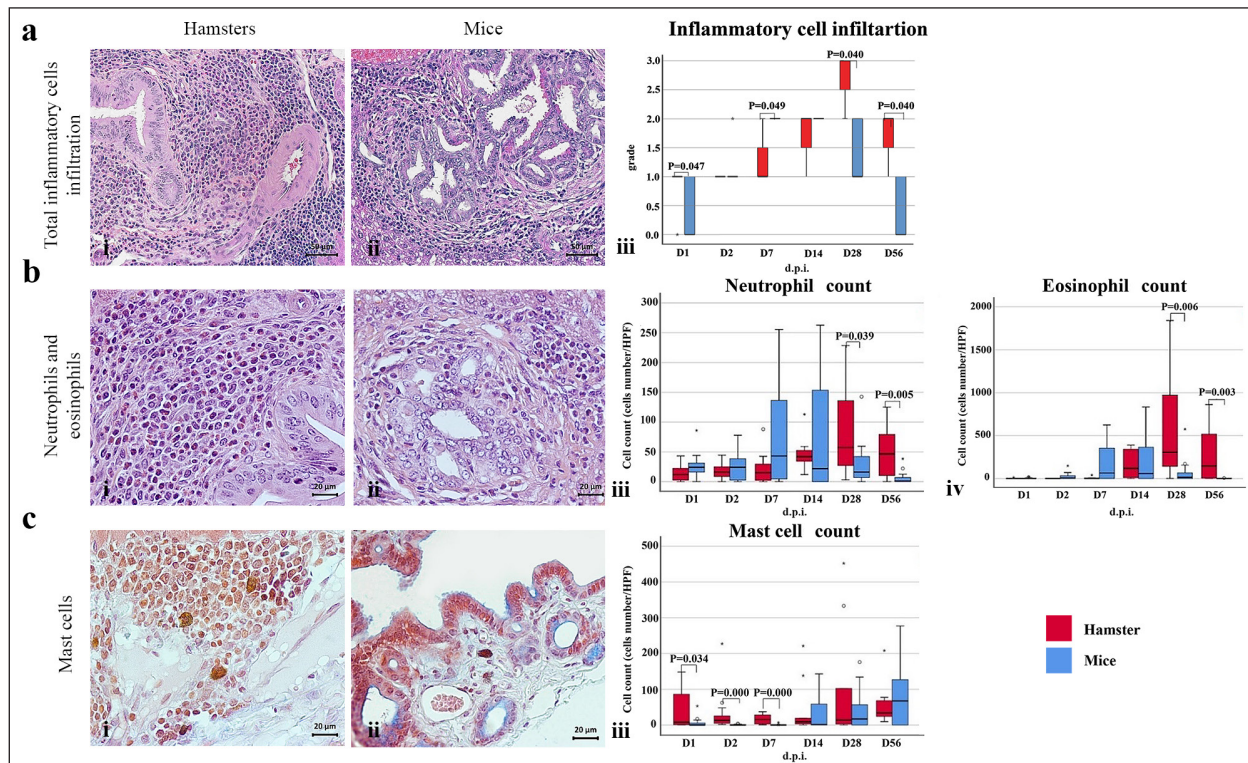


Fig. 2. The numbers of various types of inflammatory cells (total inflammatory cells, neutrophils, eosinophils, and mast cells) infiltrate the biliary area of hamsters and mice infected with *O. viverrini* from D1 to D56 p.i. The different types of inflammatory cells are located in the biliary and peri-biliary areas of hamsters (ai, bi, ci) and mice (aai, bai, cai), respectively. The graphs on the right comparatively show the grade of inflammatory cells between both groups (aiii). Early response of inflammation is present in the mice model while the chronic response is shown in a hamster model. Quantitative comparison of the individual white blood cells, including neutrophil (biii), eosinophil (biv), and mast cell (ciii) showed significantly different among OV-infected hosts ($p < 0.05$). (a–bi, a–bii = H&E; ci–cii = alcian blue-safranin O, original magnification, ai–aai = $\times 20$, scale bar depicts 50 μm ; b–ci, b–cii = $\times 40$, scale bar depicts 20 μm).

immunohistochemical techniques. In the mouse model, the population of B lymphocytes was much lower compared to the hamster model (Fig. 3ci and ii). In hamsters, B lymphocytes were present since D1 and sharply increased on D14, reaching a maximum at D28 before declining on D56. A significantly higher

amount of B lymphocytes was observed in hamsters on D1 ($p = 0.005$), D2 ($p = 0.011$), D7 ($p = 0.049$), and D14 ($p = 0.022$) (Fig. 3ciii). In contrast, in mice, B lymphocytes showed an abrupt increase on D7, a peak on D14, a decline on D28, and nearly reached ground on D56.

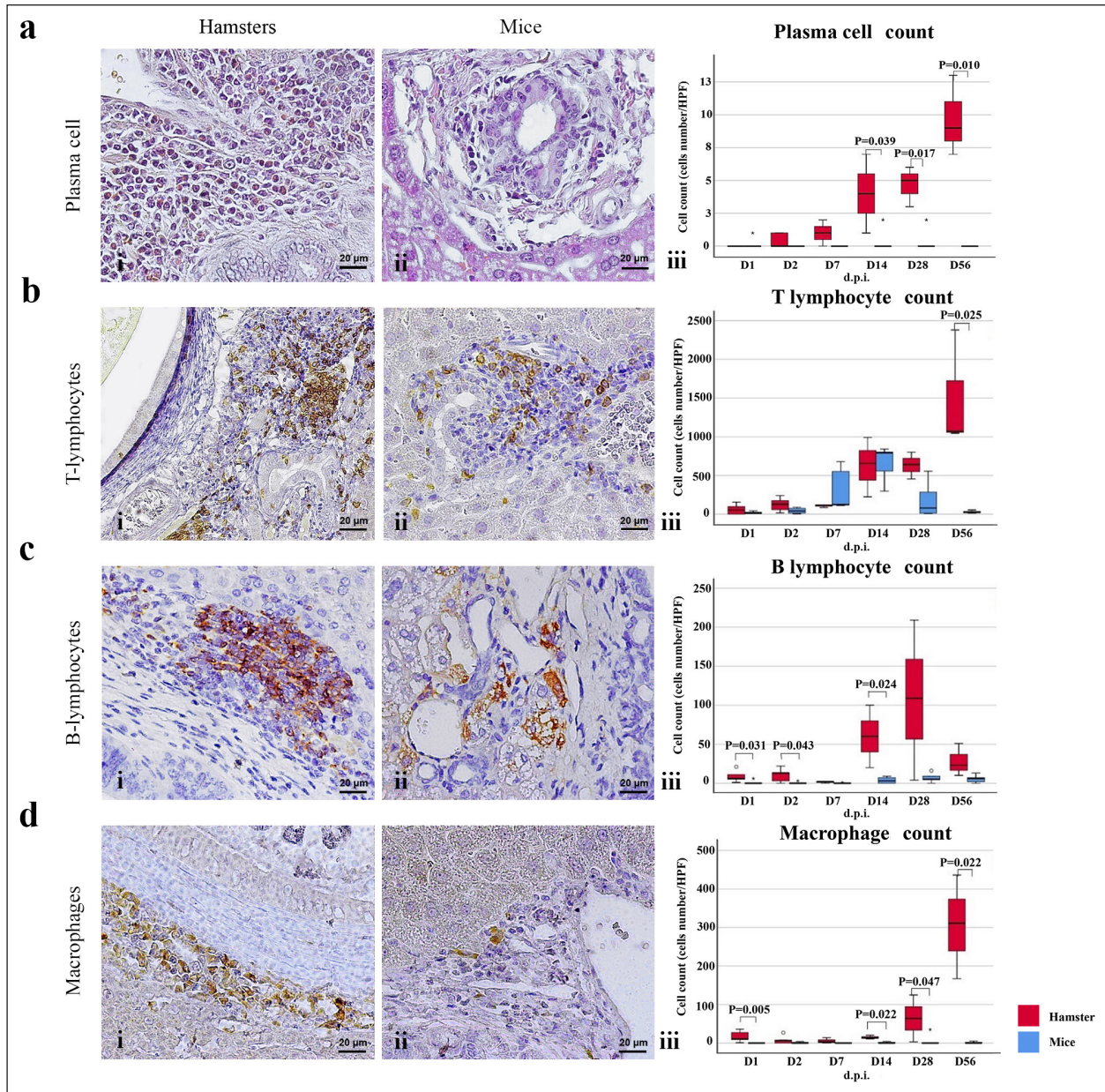


Fig. 3. Comparison of different mononuclear cell types (plasma cells, T lymphocytes, B lymphocytes, and macrophages) that infiltrate the portal area in hamsters and mice infected with *O. viverrini*. The micrographs represent the different types of inflammatory cells in hamsters (a-di) and mice (a-dii). A comparison of each individual inflammatory cell, including plasma cell (aiii), T-lymphocytes (biii), B-lymphocytes (ciiii), and macrophages (diii) are represented by graphs (right column). Mice show the early and minimal response of these mononuclear cell infiltration, while hamsters display a significantly larger and later response ($p < 0.05$) (a–diii). (ai–aii = H&E; b–di to b–dii = immunohistochemistry, original magnification, a–di, a–dii = $\times 40$, scale bar depicts 20 μm).

Infiltration of plasma cells

The number of plasma cells, which differentiate from B cells, was rarely detected in mice, whereas the cells gradually increased from D2 to D56 in hamsters (Fig. 3ai and ii). A significant difference in plasma cell numbers between mice and hamsters was found on D14 ($p = 0.039$), D28 ($p = 0.017$), and D56 ($p = 0.010$) (Fig. 3aiii).

Infiltration of macrophages

Macrophages are one of the cell types included in the mononuclear cell population. In this study, immunohistochemical techniques were used to demonstrate macrophages in general, without distinguishing between specific types. The results showed that macrophage presence was more prominent in the hamster model (Fig. 3di and ii), especially in the chronic phase on D28 and D56. The hamster model showed significantly higher macrophage infiltration than the mouse model throughout all periods ($p < 0.05$) (Fig. 3diii).

Periductal fibrosis

PDF was graded semi-quantitatively according to the criteria described in Table 1. The fibrosis was mainly observed in the first-order bile ducts where *O. viverrini* was present, but it was rarely seen in the second-order bile ducts. The fibrous tissue presented from periductal tissue of large portal areas which observed on D7 in hamsters and extended to small portal triads in chronic infection on D56 (Fig. 4). Compared to the mouse model, PDF increased significantly in D14 ($p = 0.008$).

Correlation between PDF grades and different types of inflammatory cell infiltration

Spearman's rank-order correlation was used to assess the relationship between PDF and various types of inflammatory cells infiltrating the biliary epithelium (Table 3).

Significant correlations were mostly found in the hamster group. In the hamster model, a very strong positive correlation was observed between PDF and eosinophils ($r_s = 0.806$, $p = 0.000$), T-lymphocytes ($r_s = 0.838$, $p = 0.000$), and plasma cells ($r_s = 0.876$, $p = 0.000$), with a strong positive correlation observed with neutrophils ($r_s = 0.633$, $p = 0.002$), mast cells ($r_s = 0.667$, $p = 0.001$), mononuclear cells ($r_s = 0.631$, $p = 0.002$), B-lymphocytes ($r_s = 0.520$, $p = 0.013$), and macrophages ($r_s = 0.529$, $p = 0.011$). In contrast, the PDF in the mouse model showed a strong negative correlation with neutrophils ($r_s = -0.470$, $p = 0.009$) and a moderate positive correlation with B-lymphocytes ($r_s = 0.383$, $p = 0.037$).

Proliferative lesions

Biliary epithelial proliferative lesions

The present study investigated proliferative lesions of biliary epithelial pathology, focusing on two major microscopic lesions: biliary hyperplasia and dysplasia (as shown in Fig. 4). To determine the cell proliferation activity, we performed BrdU immunohistochemistry and calculated the BrdU index. The index was compared between the models and times to assess the proliferation activity.

Biliary hyperplasia and bile duct proliferation

Histological evaluation of biliary cell proliferation was performed by grading epithelial hyperplasia in the first-order bile duct and bile duct proliferation in the second-order bile duct. Biliary hyperplasia and bile duct proliferation were categorized based on the proliferation, stratification, and mucosal folding of the biliary epithelium or the number of bile ducts per portal area, and graded as shown in Table 1. Hyperplasia was observed in both rodent models infected with OV (as shown in Fig. 4). In the mouse model, the hyperplasia of the first-order bile duct abruptly increased only on D14, while a similar increase was found in the chronic phase (D28). A higher degree of biliary hyperplasia was observed in the *O. viverrini*-infected hamster (HOV) group on days 1, 2, 28, and 56, while a higher degree of biliary hyperplasia was observed in the *O. viverrini*-infected BALB/c mouse (MOV) group on days 2, 7, and 14 (as shown in Fig. 4ai–iii). It was found that marked proliferation was rarely present in both models.

BrdU proliferation index

Semi-quantitative analysis of biliary cell proliferation by BrdU labeling was performed in immunohistochemically stained portions, where positive biliary nuclei were counted (as shown in Fig. 4) and scored as described in Table 1. In hamsters, a higher degree of BrdU index was found in the OV infection groups on D14, D28, and D56 p.i. In contrast, in mice, the higher BrdU index was found in the early period of OV infection groups, specifically on D1 and D2, which then declined in the late period. The HOV group had a significantly higher BrdU index than the MOV group ($p = 0.024$) on D28 and D56 ($p = 0.024$) p.i. On the other hand, the MOV group showed a significant increase in the BrdU index on the first day postinfection compared to the HOV group ($p = 0.005$). In addition, the MOV group had a significant increase in the BrdU index on D2 p.i. compared to the Hams OV group ($p = 0.009$) (as shown in Fig. 4).

Biliary dysplasia

Biliary dysplasia recognized by hyperplastic and hyperchromatic epithelium with infrequent mitotic figures was shown in the first-order bile ducts. Dysplasia was commonly seen in areas with active inflammation and its occurrence depended on the duration and study groups. In the mouse model, the lesion was detected earlier and peaked on D14. However, the lesion declined and disappeared at D56. In the hamster model, dysplasia appeared from D14 and increased until D56. Compared to other proliferation lesions, it was rarely seen in the early phase of infection of both animal models.

Correlation between inflammatory cell infiltration and biliary proliferative lesions

It is well-established that inflammation plays a significant role in the development of cancers. In this study, various proliferative lesions such as hyperplasia, bile duct proliferation, hyperplasia of the second order bile duct, and dysplasia were analyzed, along

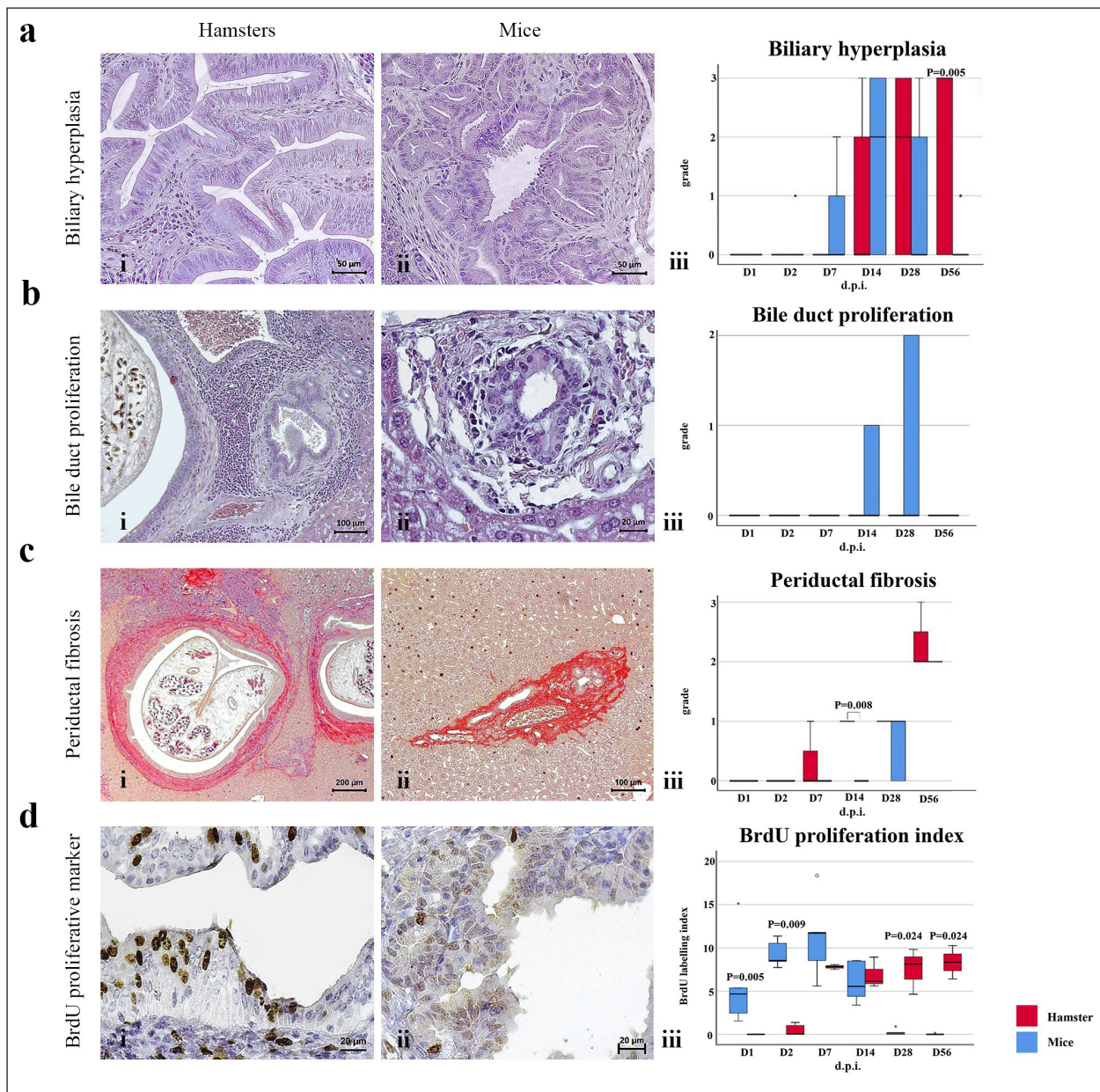


Fig. 4. Comparison of biliary proliferation lesions, PDF, and BrdU index between *O. viverrini* infected hamster and mouse models. The type of lesions and BrdU are indicated by rows A to D and the left and middle columns refers to hamster and mouse, respectively. The right column shows the comparative number of inflammatory cells of each models.

with the BrdU index, which reflects proliferation activity. Spearman's rank-order correlation was used to determine the relationship between inflammatory cell infiltration grades and these variables. The results showed a very strong positive correlation between bile duct hyperplasia and inflammatory cell infiltration grades in both the mouse and hamster models (mice $r_s = 0.707$, $p = 0.000$ and hamsters $r_s = 0.777$, $p = 0.000$). There was also a moderate positive correlation between bile duct proliferation ($r_s = 0.375$, $p = 0.041$) and the BrdU index ($r_s = 0.390$, $p = 0.033$) in the mouse

model. In the HOV group, there was a very strong and strong positive correlation with the BrdU index ($r_s = 0.678$, $p = 0.001$), respectively (Table 4). The Spearman correlation test showed a strong positive correlation between inflammatory cell infiltration and bile duct hyperplasia in both the hamster and mouse models. There was also a moderate positive correlation between bile duct proliferation and the BrdU index in the mouse model. In the hamster model, there was a very strong positive correlation with PDF and a strong positive correlation with the BrdU index. These

Table 3. Correlation between PDF grades and white blood cell counts, *p*-value from Spearman correlation test.

| Criteria; PDF grades correlate with | Mice (rs) | Mice (p-value) | Hamsters (rs) | Hamsters (p-value) |
|-------------------------------------|---------------------|----------------|--------------------|--------------------|
| Neutrophils | -0.470 ^d | 0.009 | 0.633 ^b | 0.002 |
| Eosinophils | -0.204 | 0.279 | 0.806 ^a | 0.000 |
| Mast cells | -0.327 | 0.078 | 0.667 ^b | 0.001 |
| Mononuclear cells | -0.076 | 0.690 | 0.631 ^b | 0.002 |
| T lymphocytes | -0.186 | 0.326 | 0.838 ^a | 0.000 |
| B lymphocytes | 0.383 ^c | 0.037 | 0.520 ^b | 0.013 |
| Plasma cells | -0.199 | 0.293 | 0.876 ^a | 0.000 |
| Macrophages | 0.300 | 0.107 | 0.529 ^b | 0.01 |

^a very strong positive; ^b strong positive; ^c moderate positive; ^d strong negative.

Table 4. Correlation between inflammatory cell infiltration and biliary responses in the hamster and mouse models analyzed by Spearman correlation test.

| Criteria; Inflammatory cells infiltration correlate with | Mice (rs) | Mice (p-value) | Hamsters (rs) | Hamsters (p-value) |
|--|--------------------|----------------|--------------------|--------------------|
| Bile duct hyperplasia grades | 0.707 ^a | 0.000 | 0.777 ^a | 0.000 |
| Bile duct proliferation grades | 0.375 ^c | 0.041 | - | - |
| PDF grades | -0.242 | 0.198 | 0.746 ^a | 0.000 |
| BrdU index | 0.390 ^c | 0.033 | 0.678 ^b | 0.001 |

- unavailable by Spearman correlation test; ^a very strong positive; ^b strong positive; ^c moderate positive.

findings suggest that inflammation may play a crucial role in the development of proliferative lesions and PDF in opisthorchiasis.

Discussion

Based on the susceptibility of the host immune response, two animal models were used in this study to compare the inflammatory response of the low responder or nonsusceptible host (BALB/c mouse) and high responder or susceptible host (Syrian golden hamster). Patterns of inflammatory cell infiltration to the infected liver of both animal models were observed, as well as the biliary proliferative lesions.

Regarding the status of infection, it was examined by the presence of parasite eggs in feces and the worm in the bile duct. Previous studies reported the *O. viverrini* uterus was filled with eggs after 20–23 days and eggs were detected in the feces on day 26 (Nithikathkul et al., 2007; Kaewpitoon et al., 2012). The absence of *O. viverrini* eggs in mice and their presence in hamsters from D28 to D56 in this study suggests the difference in host susceptibility to *O. viverrini* infection in these two animal models. Another supporting evidence is the presence of juvenile worms in the liver section. In the mouse model, the worm section was detected from D1 to D28 while the worm section was presented throughout the study. Noticeably, the calcified dead

worm section was also shown at D28 of the mouse model that reflecting the unsuccessful establishment of infection present in the nonsusceptible host.

Pathological study suggests that the hamster model showed a higher level of inflammatory cell infiltration compared to the mouse model, especially in the chronic phase of infection. This may be attributed to the predominant Th2 response observed in hamsters in the chronic stage of *O. viverrini* infection (Sripa et al., 2018a). The *O. viverrini* excretory and secretory products (OVES) contain various molecules that attract different inflammatory cells to migrate and accumulate around and within the bile duct, including both somatic and ES antigens. Although mice are not a common model for *O. viverrini* study, *Clonorchis sinensis* (*C. sinensis*) is a related species that has been studied. Inflammatory cells increased and peaked around 2–3 weeks postinfection before gradually declining, with Th2-mediated IL-4 involvement (Choi et al., 2003).

The initial stage of *O. viverrini* infection in hamsters involves innate immune cells, such as neutrophils, eosinophils, macrophages, and mast cells, acting as inflammatory cells (Sripa and Kaewkes, 2000a; Suyapoh et al., 2021b). Prolonged infection then stimulates the function of adaptive immune cells, such as lymphocytes and macrophages, which are involved in tissue repair (Sripa et al., 2018a; Wang et al., 2021). The initial infiltration was often seen in the first-ordered

bile ducts at early infection, and a small number of this cell type was observed in infected hamsters over the infection periods (Suyapoh *et al.*, 2021b).

Neutrophil is the inflammatory cell type that responds quickly because its activation occurs before that of other inflammatory cells such as eosinophils, mast cells, lymphocytes, and macrophages (Salao *et al.*, 2020; Peixoto *et al.*, 2021). Interestingly, mice showed higher levels of neutrophil number in the acute and subacute phases, while hamsters showed higher levels in the chronic phase. Neutrophil infiltration in this study increased earlier and higher in mice from D7–D14 and declined abruptly in D28 and D56. Hamster neutrophils raised slower, peaked on D28, and declined on D56. However, the reason for this difference is unclear, and further studies are needed to explain it.

Eosinophils are inflammatory cells that are commonly found in response to helminth infections and allergies, where they engage in IgE binding at the mast cell surface and directly affect the degranulation process (Simon *et al.*, 2020). Eosinophils secrete various substances, such as eosinophil cationic proteins, major basic proteins, and eosinophil-derived neurotoxins that are toxic to helminths. In addition, eosinophils release enzymes, cytokines, and lipid mediators that promote tissue remodeling, stimulate other cells in the immune system, and induce smooth muscle contraction, which may aid in expulsive mechanisms (Yasuda and Nakanishi, 2018; Yasuda and Kuroda, 2019). Consistent with previous studies, the number of eosinophils in *O. viverrini*-infected hamsters increased within the first month and then decreased within 60 days (Sripa and Kaewkes, 2000a; Suyapoh *et al.*, 2021b). In the mouse model in this study, the number of eosinophils in mice was noticeably higher than in hamsters on day 1. This is similar to a study in BALB/c mice infected with *C. sinensis* (Choi *et al.*, 2003). In the later phase, the level of eosinophil count in hamsters was significantly higher than that of mice at days 28 and 56. Susceptibility to the fluke infection may be linked to the regulation of IgE secretion, which is controlled by the adaptive immune response (Th2). This response is based on the production of interleukin-5 (IL-5) by Th2 cells (Uddin *et al.*, 2012).

Mast cells in the liver are predominantly found in the connective tissue surrounding the hepatic arteries, veins, and bile ducts. An increase in mast cell numbers has been observed during tissue repair processes, including fibrosis, which reflects the chronic stage (Weiskirchen *et al.*, 2019). When stimulated by IgE and antigen crosslinking, the IgE receptor Fc ϵ ER on the mast cell surface can trigger the secretion of substances from granules. Degranulation, lipid mediators, and cytokines have both direct and indirect effects on helminths (Espinosa and Valitutti, 2018; Ryan and Oghumu, 2019). Th2-dependent production of IL-4 and IL-9 is responsible for the proliferation and activation of mast cells (Koyama and Ito, 2000). The infiltration of mast

cells is predominantly detected in lamina propria and submucosa similar to the study in humans (Albert-Bayo *et al.*, 2019; Sripa and Haswell, 2021). Our study shows that the number of mast cells in mice responded particularly in the late phase. In parasitic infections, mast cells are typically found following the introduction of eosinophils in combination with IgE. However, in hamsters, mast cells are usually found both in the acute and chronic phases. This may be due to the avoiding mechanism of the living parasite suppressing the mast cell response, allowing the parasite to survive and leading to susceptibility to infection. Once chemokine is produced and released by mast cells (Gieseck *et al.*, 2018).

Mononuclear cells are a mixture of various types of cells with a single round nucleus, including lymphocytes, plasma cells, macrophages, and young cells. They are typically detected in chronic inflammation. Exposure to proinflammatory cytokines and sustained stimulation of signaling pathways generate free radicals such as reactive oxygen species (ROS) and reactive nitrogen species (RNS) from inflammatory and epithelial cells, causing oxidative damage (Chen *et al.*, 2018).

Plasma cells are typically found in the chronic phase of infection, responding to the persistence of the causative agents and contributing to the adaptive immune response. Even though mice rarely show the presence of the worms after D14, the host's immune mechanisms still respond to antigens in different ways, including the use of antibodies produced from plasma cells. The response to various antigens persists even though the parasite is rarely found, until around D56 when the number of plasma cells decreases with the repair of damaged sites. This suggests that the *O. viverrini* may be expelled from the host, leading to a reduced response mechanism. However, ES products, somatic and egg antigens were still found to contribute to a higher antibody response. In cases of chronic and heavy infection, the antibody response is significantly lower compared to mild infections due to immunosuppression (Sripa and Kaewkes, 2000b). The data from another study in our group that shows a distinct antibody profile of these two models may reflect the differences in the host's response to *O. viverrini* infection (Watakulsin *et al.*, 2023). The mouse antibody is raised earlier than the antibody in the hamster model, which may be due to differences in the period of infection and the worm's maturity. In the hamster model, the antibody abruptly increases and maintains a high level from D14–D28, which may be linked to the period of infection and worm maturity.

In the hamster model, the number of T-lymphocytes gradually increases which shows the highest response on D56. Similar to other parasitic infections, *O. viverrini* infected host has a mechanism to switch from Th1 to Th2 responses as appropriate for the chronic infection. If the immune system has an overreaction, it leads to an adjustment to reduce the response, allowing

O. viverrini to exist more easily (Butcher and Zhu, 2021; Gazzinelli-Guimaraes and Nutman, 2018). With shifting to Th2 responses in chronic infection, the immunity allows parasites to evade the host immune response (Jittimaneet et al., 2007). Our study on infected mice showed high levels of T-cells in D7 and D14. The T-lymphocytes found in mice at D14 are likely from adaptive immunity. In the chronic phase, infiltration of T-cells gradually declines, approaching the baseline. In mice infected with *C. sinensis*, elevated levels of IgE, IFN- γ , and IL-13 suggest that both Th1 and Th2 responses may be related to host susceptibility (Uddin et al., 2012). In addition, mucosal immunity also plays a role. IL-4 and IL-13 are based on Th2, responsible for stimulating goblet cells to secrete mucin, smooth muscles to contract, and epithelial cells to divide, which all help in expelling helminths from the intestines (Zhao et al., 2003; Yasuda and Nakanishi, 2018; Coakley and Harris, 2020b; Varela et al., 2022; Atagozli et al., 2023).

It is important to note that B-lymphocytes play a critical role in the humoral immune response, which involves the production of antibodies that target foreign invaders such as parasites. B-lymphocyte response may not be significantly related to differences in *O. viverrini* infection susceptibility. This is because of the result of the immune response to humoral immunity which is differentiated from B-lymphocytes to plasma cells. IL-4 function is based on Th2. They are responsible for signaling B-lymphocytes to produce IgE, and helminth infections simultaneously activate regulatory T lymphocytes, helping to prevent excessive tissue destruction. Alternately, at the same time suppressing this immunity allows the helminths to live longer in the host (Junttila, 2018).

Due to the prolonged infection, hamsters exhibit a wider range of damages in the inflamed area compared to mice. The level of macrophages in the hamster model is higher than that of the mouse model, indicating that the process of tissue damage is less likely in mice. In addition, *O. viverrini* eggs were not detected in the mouse model, while the egg granulomas were found in the chronic phases of all experiments in hamsters. Macrophages were detected among the granulomatous tissue, consistent with previous studies (Sripa and Kaewkes, 2000a; Lvova et al., 2012). During *O. viverrini* infection, macrophages with high phagocytic and proteolytic activities, along with elevated ROS production, can promote tissue damage leading to PDF (Salao et al., 2019). IL-4 and IL-13, based on Th2 response, stimulate macrophages to become alternatively activated macrophages (AAMs) or M2, which secrete mediators with a slow-killing effect on helminths (Yasuda and Nakanishi, 2018). Simultaneously, AAM stimulates tissue repair, similar to wound healing and repair (Rolot and Dewals, 2018; Coakley and Harris, 2020a). In addition, macrophages secrete IL-10 and TGF-beta, which regulate

inflammation and prevent it from becoming excessive (Junttila, 2018; Caputa et al., 2019), as observed in our results where inflammation decreased.

Regarding the PDF and types of inflammatory cells, the results suggest that the two animal models are different. In the hamster model, the PDF grade relates to all inflammatory cells, with a very strong correlation to eosinophils, T-lymphocytes, and plasma cells, and a strong positive correlation with other inflammatory cells (neutrophils, mast cells, mononuclear cells, B-lymphocytes, and macrophages). Recently, a study in humans suggests that the function of circulating neutrophils is enhanced and more activated in humans with advanced PDF (Salao et al., 2020). Our study in the nonsusceptible host, the mouse model shows a strong negative correlation with neutrophils but a moderate positive correlation with B lymphocytes. The PDF, especially advanced PDF (APF), is believed to be a precancerous lesion in human CCA. Studies of cytokines in human opisthorchiasis have shown that IL-6 is related to APF (Sripa et al., 2009). Later, *in vitro* cytokine stimulation of OVES revealed that *O. viverrini* could induce IL-4, IL-5, and IL-13 responses that are related to fibrosis development (Surapaitoon et al., 2017a, 2017b). The fibrosis in chronic *O. viverrini* infection is composed of types I and III collagens (Prakobwong et al., 2009). This suggests that the increased amount of these collagens in the portal tract and along the peri-sinusoid space, not the basement membrane around the bile duct or vessels (Karsdal et al., 2020).

A correlation study of inflammatory cell infiltration with biliary responses suggests a strong positive correlation with bile duct hyperplasia in both the hamster and mouse models and a moderate positive correlation with bile duct proliferation in mice. The cell proliferation marker, the BrdU index, supports these findings. It shows a strong correlation in the hamster model and a moderate correlation in the mouse model. These findings suggest that inflammation may play a crucial role in the development of proliferative lesions and PDF in opisthorchiasis. The studies of mitogenic molecules in OVES such as granulins and inflammatory response revealed that the molecules promote cell proliferation and play an important role in CCA development both *in vitro* and *in vivo* (Smout et al., 2009; Chaiyadet et al., 2022).

Conclusion

Both rodent models are useful for studying the host susceptibility of opisthorchiasis. As a nonsusceptible animal model, BALB/c mice respond to *O. viverrini* infection earlier and then decline quicker than in hamsters, a susceptible animal model. In the meantime, most of the inflammatory cell types show a higher response to the *O. viverrini* infection in the later phase in golden Syrian hamsters. Correlation between the precancerous lesion, PDF, and types of inflammatory

cells in the hamster model suggests the linkage of inflammatory cells and this precancerous lesion. The findings suggest that inflammatory cell response probably plays a crucial role in host susceptibility and biliary cell proliferation in opisthorchiasis pathogenesis. This could be applied to the effective prevention of *O. viverrini*-associated CCA.

Acknowledgment

This study was financially supported by Research and Graduate Studies, Faculty of Veterinary Medicine, Khon Kaen University (Research Program Fiscal Year 2020); Khon Kaen University Annual Fund Year 2019–2020. The authors would like to thank Mr. Suwit Balthaisong for sample collection assistance.

Author contributions

Conceptualization, ST; Methodology, TT, ST, WDW; Validation, ST, WS; Formal Analysis, TT, PS, ST, PT; Investigation, TT, ST; Resources, TT, ST, SS, PS; KS Writing–Original Draft Preparation, TT, ST; Writing–Review and Editing, ST, PT, WS; Supervision and Editing, ST, PT. All authors have read and agreed to the submitted version of the manuscript.

Conflict of interest

The authors declare there are no conflicts of interest.

Funding

Research and Graduate Studies, Faculty of Veterinary Medicine, Khon Kaen University (Research Program Fiscal Year 2020); Khon Kaen University Annual Fund Year 2019–2020.

Data availability

All data supporting the findings of this study are available within the manuscript.

References

- Albert-Bayo, M., Paracuellos, I., Gonzalez-Castro, A.M., Rodriguez-Urrutia, A., Rodriguez-Lagunas, M.J., Alonso-Cotoner, C., Santos, J. and Vicario, M. 2019. Intestinal mucosal mast cells: key modulators of barrier function and homeostasis. *Cells* 8, 135.
- Atagozli, T., Elliott, D.E. and Ince, M.N. 2023. Helminth lessons in inflammatory bowel diseases (IBD). *Biomedicines* 11, 1200.
- Boonmars, T., Boonjaraspinyo, S. and Kaewsamut, B. 2009. Animal models for *Opisthorchis viverrini* infection. *Parasitol. Res.* 104, 701–703.
- Butcher, M.J. and Zhu, J. 2021. Recent advances in understanding the Th1/Th2 effector choice. *Fac. Rev.* 10, 30.
- Caputa, G., Flachsmann, L.J. and Cameron, A.M. 2019. Macrophage metabolism: a wound-healing perspective. *Immunol. Cell Biol.* 97, 268–278.
- Chaiyadet, S., Tangkawattana, S., Smout, M.J., Ittiprasert, W., Mann, V.H., Deenonpoe, R., Arunsan, P., Loukas, A., Brindley, P.J. and Laha, T. 2022. Knockout of liver fluke granulin, *Ov-grn-1*, impedes malignant transformation during chronic infection with *Opisthorchis viverrini*. *PLoS Pathog.* 18, e1010839.
- Chen, L., Deng, H., Cui, H., Fang, J., Zuo, Z., Deng, J., Li, Y., Wang, X. and Zhao, L. 2018. Inflammatory responses and inflammation-associated diseases in organs. *Oncotarget* 9, 7204–7218.
- Choi, Y.K., Yoon, B.I., Won, Y.S., Lee, C.H., Hyun, B.H., Kim, H.C., Oh, G.T. and Kim, D.Y. 2003. Cytokine responses in mice infected with *Clonorchis sinensis*. *Parasitol. Res.* 91, 87–93.
- Coakley, G. and Harris, N.L. 2020a. Interactions between macrophages and helminths. *Parasite Immunol.* 42, e12717.
- Coakley, G. and Harris, N.L. 2020b. The intestinal epithelium at the forefront of host–helminth interactions. *Trends Parasitol.* 36, 761–772.
- Espinosa, E. and Valitutti, S. 2018. New roles and controls of mast cells. *Curr. Opin. Immunol.* 50, 39–47.
- Gazzinelli-Guimaraes, P.H. and Nutman, T.B. 2018. Helminth parasites and immune regulation. *F1000 Res.* 7, F1000 Faculty Rev-1685.
- Gieseck, R.L., 3rd, Wilson, M.S. and Wynn, T.A. 2018. Type 2 immunity in tissue repair and fibrosis. *Nat. Rev. Immunol.* 18, 62–76.
- Grigorev, I.P. and Korzhevskii, D.E. 2021. Modern imaging technologies of mast cells for biology and medicine (Review). *Sovrem Tekhnologii Med.* 13, 93–107.
- Ishak, K., Baptista, A., Bianchi, L., Callea, F., De Groote, J., Gudat, F., Denk, H., Desmet, V., Korb, G. and MacSween, R.N. 1995. Histological grading and staging of chronic hepatitis. *J. Hepatol.* 22, 696–699.
- Jittimane, J., Sermswan, R.W., Puapairoj, A., Maleewong, W. and Wongratanacheewin, S. 2007. Cytokine expression in hamsters experimentally infected with *Opisthorchis viverrini*. *Parasite Immunol.* 29, 159–167.
- Junttila, I.S. 2018. Tuning the cytokine responses: an update on interleukin (IL)-4 and IL-13 receptor complexes. *Front. Immunol.* 9, 888.
- Kaewkes, S., Elkins, D.B., Sithithaworn, P. and Haswell-Elkins, M.R. 1991. Comparative studies on the morphology of the eggs of *Opisthorchis viverrini* and lecithodendriid trematodes. *Southeast Asian J. Trop. Med. Public Health* 22, 623–630.
- Kaewpitoon, N., Kaewpitoon, S.J., Ueng-arporn, N., Rujirakul, R., Churproong, S., Matrakool, L., Auiwatanagul, S. and Sripan, B. 2012. Carcinogenic human liver fluke: current status of *Opisthorchis viverrini* metacercariae in Nakhon Ratchasima, Thailand. *Asian Pac. J. Cancer Prev.* 13, 1235–1240.
- Karsdal, M.A., Daniels, S.J., Holm Nielsen, S., Bager, C., Rasmussen, D.G.K., Loomba, R., Surabattula, R., Villesen, I.F., Luo, Y., Shevell, D., Gudmann, N.S., Nielsen, M.J., George, J., Christian, R.,

- Leeming, D.J. and Schuppan, D. 2020. Collagen biology and non-invasive biomarkers of liver fibrosis. *Liver Int.* 40, 736–750.
- Kopolrat, K.Y., Singthong, S., Khuntikeo, N., Loilome, W., Worasith, C., Homwong, C., Wangboon, C., Yasaka, P., Eamudomkarn, C., Pitaksakulrat, O., Tonkhamhak, K., Paeyo, A., Crellen, T., Sithithaworn, J. and Sithithaworn, P. 2022. Performance of Mini Parasep((R)) SF stool concentrator kit, Kato-Katz, and formalin-ethyl acetate concentration methods for diagnosis of opisthorchiasis in Northeast Thailand. *Parasit. Vectors* 15, 234.
- Koyama, K. and Ito, Y. 2000. Mucosal mast cell responses are not required for protection against infection with the murine nematode parasite *Trichuris muris*. *Parasite Immunol.* 22, 13–20.
- Lvova, M.N., Tangkawattana, S., Balthaisong, S., Katokhin, A.V., Mordvinov, V.A. and Sripa, B. 2012. Comparative histopathology of *Opisthorchis felinus* and *Opisthorchis viverrini* in a hamster model: an implication of high pathogenicity of the European liver fluke. *Parasitol. Int.* 61, 167–172.
- Mairiang, E. 2017. Ultrasonographic features of hepatobiliary pathology in opisthorchiasis and opisthorchiasis-associated cholangiocarcinoma. *Parasitol. Int.* 66, 378–382.
- Nithikathkul, C., Tesana, S., Sithithaworn, P. and Balakanich, S. 2007. Early stage biliary and intrahepatic migration of *Opisthorchis viverrini* in the golden hamster. *J. Helminthol.* 81, 39–41.
- Peixoto, R., Silva, L.M.R., Lopez-Osorio, S., Zhou, E., Gartner, U., Conejeros, I., Taubert, A. and Hermosilla, C. 2021. *Fasciola hepatica* induces weak NETosis and low production of intra- and extracellular ROS in exposed bovine polymorphonuclear neutrophils. *Dev. Comp. Immunol.* 114, 103787.
- Pinto, C., Giordano, D.M., Maroni, L. and Marzoni, M. 2018. Role of inflammation and proinflammatory cytokines in cholangiocyte pathophysiology. *Biochim. Biophys. Acta Mol. Basis. Dis.* 1864, 1270–1278.
- Prakobwong, S., Pinlaor, S., Yongvanit, P., Sithithaworn, P., Pairojkul, C. and Hiraku, Y. 2009. Time profiles of the expression of metalloproteinases, tissue inhibitors of metalloproteinases, cytokines and collagens in hamsters infected with *Opisthorchis viverrini* with special reference to peribiliary fibrosis and liver injury. *Int. J. Parasitol.* 39, 825–835.
- Pruksapanich, P., Piyachaturawat, P., Aumpansub, P., Ridditid, W., Chaiteerakij, R. and Rerknimitr, R. 2018. Liver fluke-associated biliary tract cancer. *Gut Liver* 12, 236–245.
- Rolot, M. and Dewals, B.G. 2018. Macrophage activation and functions during helminth infection: recent advances from the laboratory mouse. *J. Immunol. Res.* 2018, 2790627.
- Ryan, N.M. and Oghumu, S. 2019. Role of mast cells in the generation of a T-helper type 2 dominated anti-helminth immune response. *Biosci. Rep.* 39, BSR20181771.
- Salao, K., Spofford, E.M., Price, C., Mairiang, E., Suttiaprapa, S., Wright, H.L., Sripa, B. and Edwards, S.W. 2020. Enhanced neutrophil functions during *Opisthorchis viverrini* infections and correlation with advanced periductal fibrosis. *Int. J. Parasitol.* 50, 145–152.
- Salao, K., Watakulsin, K., Mairiang, E., Suttiaprapa, S., Tangkawattana, S., Edwards, S.W. and Sripa, B. 2019. High macrophage activities are associated with advanced periductal fibrosis in chronic *Opisthorchis viverrini* infection. *Parasite Immunol.* 41, e12603.
- Sanpool, O., Aung, W.P.P., Rodpai, R., Maleewong, W. and Intapan, P.M. 2018. Human liver fluke *Opisthorchis viverrini* (Trematoda, Opisthorchiidae) in Central Myanmar: new records of adults and metacercariae identified by morphology and molecular analysis. *Acta Trop.* 185, 149–155.
- Sharma, S., Das, P., Dattagupta, S., Kumar, L. and Gupta, D.K. 2011. Liver and portal histopathological correlation with age and survival in extra hepatic biliary atresia. *Pediatr. Surg. Int.* 27, 451–461.
- Simon, H.U., Yousefi, S., Germic, N., Arnold, I.C., Haczk, A., Karaulov, A.V., Simon, D. and Rosenberg, H.F. 2020. The cellular functions of eosinophils: Collegium Internationale Allergologicum (CIA) update 2020. *Int. Arch. Allergy Immunol.* 181, 11–23.
- Sirivisoot, S., Teewasutrakul, P., Techangamsuwan, S., Tangkawattana, S. and Rungsipipat, A. 2018. Monitoring minimal residual disease in canine lymphomas treated with modified L-COP or L-CHOP protocols. *Acta Vet. Hung.* 66, 66–84.
- Smout, M.J., Laha, T., Mulvenna, J., Sripa, B., Suttiaprapa, S., Jones, A., Brindley, P.J. and Loukas, A. 2009. A granulins-like growth factor secreted by the carcinogenic liver fluke, *Opisthorchis viverrini*, promotes proliferation of host cells. *PLoS Pathog.* 5, e1000611.
- Sripa, B. and Haswell, M.R. 2021. Mast cell hyperplasia in *Opisthorchis viverrini*-associated cholecystitis. *Parasitol. Res.* 120, 373–376.
- Sripa, B., Jumnainsong, A., Tangkawattana, S. and Haswell, M.R. 2018a. Immune response to *Opisthorchis viverrini* Infection and Its role in pathology. *Adv. Parasitol.* 102, 73–95.
- Sripa, B. and Kaewkes, S. 2000a. Localisation of parasite antigens and inflammatory responses in experimental opisthorchiasis. *Int. J. Parasitol.* 30, 735–740.
- Sripa, B. and Kaewkes, S. 2000b. Relationship between parasite-specific antibody responses and intensity

- of *Opisthorchis viverrini* infection in hamsters. *Parasite Immunol.* 22, 139–145.
- Sripa, B., Mairiang, E., Thinkhamrop, B., Laha, T., Kaewkes, S., Sithithaworn, P., Tessana, S., Loukas, A., Brindley, P.J. and Bethony, J.M. 2009. Advanced periductal fibrosis from infection with the carcinogenic human liver fluke *Opisthorchis viverrini* correlates with elevated levels of interleukin-6. *Hepatology* 50, 1273–1281.
- Sripa, B., Tangkawattana, S. and Brindley, P.J. 2018b. Update on pathogenesis of Opisthorchiasis and cholangiocarcinoma. *Adv Parasitol.* 102, 97–113.
- Surapaitoon, A., Suttiaprapa, S., Khuntikeo, N., Pairojkul, C. and Sripa, B. 2017a. Cytokine profiles in *Opisthorchis viverrini* stimulated peripheral blood mononuclear cells from cholangiocarcinoma patients. *Parasitol. Int.* 66, 889–892.
- Surapaitoon, A., Suttiaprapa, S., Mairiang, E., Khuntikeo, N., Pairojkul, C., Bethony, J., Brindley, P.J. and Sripa, B. 2017b. Subsets of inflammatory cytokine gene polymorphisms are associated with risk of carcinogenic liver fluke *Opisthorchis viverrini*-associated advanced periductal fibrosis and cholangiocarcinoma. *Korean J. Parasitol.* 55, 295–304.
- Suyapoh, W., Tangkawattana, S., Suttiaprapa, S., Punyapornwithaya, V., Tangkawattana, P. and Sripa, B. 2021a. Synergistic effects of cagA+ *Helicobacter pylori* co-infected with *Opisthorchis viverrini* on hepatobiliary pathology in hamsters. *Acta Trop.* 213, 105740.
- Suyapoh, W., Tirnitz-Parker, J.E.E., Tangkawattana, S., Suttiaprapa, S. and Sripa, B. 2021b. Biliary migration, colonization, and pathogenesis of *O. viverrini* co-infected with CagA+ *Helicobacter pylori*. *Pathogens* 10, 1089.
- Uddin, M.H., Li, S., Bae, Y.M., Choi, M.H. and Hong, S.T. 2012. Strain variation in the susceptibility and immune response to *Clonorchis sinensis* infection in mice. *Parasitol. Int.* 61, 118–123.
- Upontain, S., Sereerak, P., Laha, T., Sripa, B., Tangkawattana, P., Brindley, P.J. and Tangkawattana, S. 2018. Granulin expression in hamsters during *Opisthorchis viverrini* infection-induced cholangiocarcinogenesis. *Asian Pac. J. Cancer Prev.* 19, 2437–2445.
- Varela, F., Symowski, C., Pollock, J., Wirtz, S. and Voehringer, D. 2022. IL-4/IL-13-producing ILC2s are required for timely control of intestinal helminth infection in mice. *Eur. J. Immunol.* 52, 1925–1933.
- Wang, N., Bai, X., Jin, X., Tang, B., Yang, Y., Sun, Q., Li, S., Wang, C., Chang, Q., Liu, M. and Liu, X. 2021. The dynamics of select cellular responses and cytokine expression profiles in mice infected with juvenile *Clonorchis sinensis*. *Acta Trop.* 217, 105852.
- Watakulsin, K., Surapaitoon, A., Ulag, L.H., Kaing, S., Suyapoh, W., Saichua, P., Salao, K., Tangkawattana, S. and Suttiaprapa, S. 2023. Distinct antibody response in susceptible and non-susceptible hosts of the carcinogenic liver fluke *Opisthorchis viverrini* infection. *Parasitology* 150, 653–660.
- Weiskirchen, R., Meurer, S.K., Liedtke, C. and Huber, M. 2019. Mast cells in liver fibrogenesis. *Cells* 8, 1429.
- Wonkchalee, O., Boonmars, T., Kaewkes, S., Chamgramol, Y., Aromdee, C., Wu, Z., Juasook, A., Sudsarn, P., Boonjaraspinyo, S. and Pairojkul, C. 2012. Comparative studies on animal models for *Opisthorchis viverrini* infection: host interaction through susceptibility and pathology. *Parasitol. Res.* 110, 1213–1223.
- Yasuda, K. and Kuroda, E. 2019. Role of eosinophils in protective immunity against secondary nematode infections. *Immunol. Med.* 42, 148–155.
- Yasuda, K. and Nakanishi, K. 2018. Host responses to intestinal nematodes. *Int. Immunol.* 30, 93–102.
- Zhao, A., McDermott, J., Urban, J.F., Jr., Gause, W., Madden, K.B., Yeung, K.A., Morris, S.C., Finkelman, F.D. and Shea-Donohue, T. 2003. Dependence of IL-4, IL-13, and nematode-induced alterations in murine small intestinal smooth muscle contractility on Stat6 and enteric nerves. *J. Immunol.* 171, 948–954.
- Zhao, S.X., Li, W.C., Fu, N., Zhou, G.D., Liu, S.H., Jiang, L.N., Zhang, Y.G., Wang, R.Q., Nan, Y.M. and Zhao, J.M. 2020. Emperipolesis mediated by CD8(+) T cells correlates with biliary epithelia cell injury in primary biliary cholangitis. *J. Cell Mol. Med.* 24, 1268–1275.

Supplementary Materials

Table S1. Comparison of the mean rank of the infiltrating cell counts from all locations at different postinfection days (D) between the OV-infected hamsters and control groups.

| Infiltrating cells | Groups | D1 | | D2 | | D7 | | D14 | | D28 | | D56 | | | | | | | | | | | |
|--------------------------------|----------|----|----|--------------|----|----|--------------|-----|---|--------------|----|-----|--------------|----|---|--------------|----|---|--|----|---|--|--------------|
| | | MR | N | p-value* | MR | N | p-value* | MR | N | p-value* | MR | N | p-value* | MR | N | p-value* | | | | | | | |
| Neutrophils | Infected | 20 | 15 | | 19 | 15 | | 10 | 9 | | 12 | 9 | | 11 | 9 | | 10 | 9 | | 10 | 9 | | 0.033 |
| | Control | 11 | 15 | 0.008 | 12 | 15 | 0.021 | 9 | 9 | 0.625 | 7 | 9 | 0.042 | 4 | 6 | 0.006 | 5 | 6 | | 5 | 6 | | |
| Eosinophils | Infected | 17 | 15 | | 17 | 15 | | 11 | 9 | | 12 | 9 | | 11 | 9 | | 10 | 9 | | 10 | 9 | | 0.012 |
| | Control | 14 | 15 | 0.316 | 14 | 15 | 0.429 | 8 | 9 | 0.254 | 7 | 9 | 0.040 | 4 | 6 | 0.005 | 5 | 6 | | 5 | 6 | | |
| Mast cells | Infected | 21 | 15 | | 23 | 15 | | 14 | 9 | | 13 | 9 | | 10 | 9 | | 11 | 9 | | 11 | 9 | | 0.001 |
| | Control | 11 | 15 | 0.001 | 8 | 15 | 0.000 | 5 | 9 | 0.001 | 6 | 9 | 0.005 | 4 | 6 | 0.007 | 4 | 6 | | 4 | 6 | | |
| Mononuclear cells | Infected | 18 | 15 | | 18 | 15 | | 9 | 9 | | 13 | 9 | | 10 | 9 | | 11 | 9 | | 11 | 9 | | 0.001 |
| | Control | 13 | 15 | 0.105 | 13 | 15 | 0.125 | 11 | 9 | 0.427 | 6 | 9 | 0.009 | 6 | 6 | 0.077 | 4 | 6 | | 4 | 6 | | |
| B cells | Infected | 8 | 5 | | 8 | 5 | | 5 | 3 | | 5 | 3 | | 4 | 3 | | 4 | 3 | | 4 | 3 | | 0.076 |
| | Control | 3 | 5 | 0.005 | 4 | 5 | 0.018 | 3 | 3 | 0.114 | 2 | 3 | 0.037 | 2 | 2 | 0.076 | 2 | 2 | | 2 | 2 | | |
| Inflammatory cell infiltration | Infected | 22 | 15 | | 19 | 15 | | 10 | 9 | | 13 | 9 | | 11 | 9 | | 11 | 9 | | 11 | 9 | | 0.001 |
| | Control | 10 | 15 | 0.000 | 12 | 15 | 0.015 | 9 | 9 | 0.791 | 6 | 9 | 0.009 | 4 | 6 | 0.007 | 4 | 6 | | 4 | 6 | | |
| Hyperplasia Grades | Infected | 16 | 15 | | 16 | 15 | | 10 | 9 | | 12 | 9 | | 10 | 9 | | 10 | 9 | | 10 | 9 | | 0.013 |
| | Control | 16 | 15 | 1.000 | 16 | 15 | 1.000 | 10 | 9 | 1.000 | 8 | 9 | 0.029 | 5 | 6 | 0.015 | 5 | 6 | | 5 | 6 | | |
| Dysplasia Grades | Infected | 16 | 15 | | 16 | 15 | | 10 | 9 | | 10 | 9 | | 8 | 9 | | 7 | 9 | | 7 | 9 | | 0.072 |
| | Control | 16 | 15 | 1.000 | 16 | 15 | 1.000 | 10 | 9 | 1.000 | 10 | 9 | 1.000 | 8 | 6 | 1.000 | 10 | 6 | | 10 | 6 | | |
| Proliferation Grades | Infected | 6 | 5 | | 6 | 5 | | 4 | 3 | | 4 | 3 | | 3 | 3 | | 3 | 3 | | 3 | 3 | | 1.000 |
| | Control | 6 | 5 | 1.000 | 6 | 5 | 1.000 | 4 | 3 | 1.000 | 4 | 3 | 1.000 | 3 | 2 | 1.000 | 3 | 2 | | 3 | 2 | | |
| PDF | Infected | 6 | 5 | | 6 | 5 | | 4 | 3 | | 5 | 3 | | 4 | 3 | | 4 | 3 | | 4 | 3 | | 0.068 |
| | Control | 6 | 5 | 1.000 | 6 | 5 | 1.000 | 3 | 3 | 0.317 | 2 | 3 | 0.025 | 2 | 2 | 0.046 | 2 | 2 | | 2 | 2 | | |

*p-value from Mann–Whitney test. p value less than 0.05 is statistically significant. N from X3 locations (gallbladder, common bile duct, and intrahepatic bile duct); MR: mean rank.

Table S2. Comparison of the mean rank and median interquartile range (IQR) of the infiltrating cell counts from all locations and postinfection days between the OV-infected and control groups of hamster model and mouse model.

| Infiltrating cells | OV-Infected group (<i>n</i> ** = 66) | | Control group (<i>n</i> ** = 60) | | <i>p</i> -value* |
|--------------------|--|--------------|--------------------------------------|--------------|------------------|
| | Mean rank | Median (IQR) | Mean rank | Median (IQR) | |
| Hamster model | | | | | |
| Neutrophils | 79 | 21 (7–45) | 46 | 2 (0–13) | 0.000 |
| Eosinophils | 75 | 3 (0–142) | 51 | 0 (0–2) | 0.000 |
| Mast cells | 89 | 15 (3–48) | 36 | 0 (0–0) | 0.000 |
| Mononuclear cells | 76 | 89 (26–190) | 50 | 38 (9–70) | 0.000 |
| B cells | 31 | 12 (3–30) | 12 | 0 (0–0) | 0.000 |
| Mouse model | | | | | |
| Neutrophils | 114 | 19 (1–43) | 59 | 0 (0–3) | 0.000 |
| Eosinophils | 112 | 2 (0–63) | 62 | 0 (0–0) | 0.000 |
| Mast cells | 103 | 0 (0–29) | 71 | 0 (0–0) | 0.000 |
| Mononuclear cells | 112 | 46 (9–106) | 62 | 2 (0–19) | 0.000 |
| B cells | 36 | 0 (0–6) | 23 | 0 (0–0) | 0.000 |

p*-value from Mann–Whitney test. *p* value less than 0.05 is statistically significant. *n* from X3 location (gallbladder, common bile duct, and intrahepatic bile duct).